Mutations at the Alphavirus E2/E1 inter-dimer interface have host-specific phenotypes

Sophia C. Ren[1,±], Shefah A. Qazi[1,±], Brian Towell[2], Joseph CY Wang[3], and Suchetana Mukhopadhyay[1,*]

[1]Department of Biology, [2]Molecular and Cellular Biochemistry, Indiana University, Bloomington, IN 47405, and [3]Department of Microbiology and Immunology, Penn State College of Medicine, Hershey, PA 17033

Running Title: Contacts between E1-E2 heterodimers affect particle assembly

[±]These authors contributed equally to this work
[2]Current address: LabCorp Drug Development. Indianapolis, IN

*Corresponding author: 212 S. Hawthorne Drive, Bloomington, IN 47405.
812-856-3686 (Phone)
sumukhop@indiana.edu (Email)

ABSTRACT

Alphaviruses are enveloped viruses that are transmitted by an arthropod vector to vertebrate hosts. Alphaviruses have glycoprotein spikes on their particle surface which are essential for viral entry. Each of the 80 spikes on the surface of an alphavirus particle consists of a trimer of E2-E1 heterodimers. Two types of interactions make up the spikes: (1) interactions between E2 and E1 of the same heterodimer called intra-dimer contacts, and (2) inter-dimer interactions between E2 of one heterodimer and E1 of the adjacent heterodimer (called E1'). We hypothesized that the inter-dimer interactions are essential for trimerization of the E2-E1 heterodimers into a functional spike. In this work, we made a mutant virus where we replaced six inter-dimeric residues in Sindbis virus (WT SINV) with those from Chikungunya virus (CHIKV); the mutant is called CPB. CPB grew slower and to lower levels than WT SINV in mammalian cells, but not mosquito cells. When CPB virus was purified from mammalian cells, particles showed reduced amounts of glycoproteins relative to capsid protein, and defects in particle morphology compared to mosquito cells. CPB transported glycoproteins to the plasma membrane in similar amounts to WT SINV in mammalian cells. Two revertants, E2-H333N and E1-S247L, restored particle assembly to different degrees. The viruses were visualized by cryo-EM. We determined that the spikes of CPB had a different conformation than WT SINV or the revertants. We conclude that the inter-dimer mutant, CPB, has host-dependent defects in spike trimerization and/or particle budding in mammalian cells.

IMPORTANCE

Alphaviruses, which can cause disease when spread to humans by mosquitoes, have been classified as an emerging pathogen with a global distribution. The spikes on the surface of the alphavirus particle are absolutely required for the virus to enter a new host cell and initiate an infection. Using a structure-guided approach, we made a mutant virus that alters spike assembly in mammalian cells but not mosquito cells. This is important because it identifies a region in the spike that could be a target for antiviral drug design.

INTRODUCTION

Alphaviruses are most commonly transmitted by arthropod vectors, usually mosquitoes, to vertebrate hosts, including humans, birds, and horses (1, 2). While a majority of alphaviruses have an arthropod vector, a group of alphaviruses have been identified to transmit only between invertebrates (3), and others use a different vector to infect aquatic animals (4). Therefore, for an alphavirus to complete its infection cycle, it must be able to assemble particles in all of these host environments. Virus infection must rely on different host factors since the same viral proteins are synthesized.

The alphavirus genome consists of four nonstructural proteins and six structural proteins, which are required for viral genome replication and particle assembly, respectively (1, 2, 5, 6). The alphavirus particle consists of an inner nucleocapsid core, a host-derived lipid membrane, and 80 trimeric spikes on the surface of the virion (7). The spikes are trimers of E2-E1 heterodimers with each heterodimer forming the edge of a triangular spike. Both the E2 and E1 proteins each contain a single transmembrane domain and are embedded within the viral membrane. The endodomain of E2 interacts with the capsid protein in the core in a 1:1 ratio (8-12). Thus, the E2 protein transits the entire particle and helps align the core and the spikes, a unique feature of alphaviruses compared to other enveloped viruses (7).

Alphavirus spike assembly is a highly regulated process that depends on specific interactions between the viral proteins and host factors. The structural proteins are translated as a capsid-E3-E2-6K-E1 polyprotein (or capsid-E3-E2-TF when frameshifting occurs). Capsid is autoproteolytically cleaved from the rest of the polyprotein (13). E3 serves as the signal sequence to translocate the rest of the

polyprotein into the endoplasmic reticulum (ER) (14, 15), where the cellular enzyme signalase cleaves the polyprotein into E3-E2 (also known as pE2 or P62), 6K, and E1 (16, 17). When programmed ribosomal frameshifting occurs the protein pE2 and TF are translated (5). In mammalian cells, the ER chaperones Erp57 and calnexin/calreticulin regulate the folding and disulfide bond formation of E2 (18-20), and BiP and protein disulfide isomerase do the same for E1 (18-22). pE2 and E1 form heterodimers within the ER, before transiting to the Golgi where trimerization of the stable spike complex is predicted to occur. Glycosylation of E2 and E1 occur in the ER and Golgi. In the ER and Golgi, there is a slight decrease in pH and the E3 proteins acts as a clamp and prevents low pH mediated dissociation of the E2-E1 heterodimer (23-25). These spikes in the stable conformation are transported to the plasma membrane through the host secretory system. In the late secretory pathway, the cellular enzyme furin cleaves E3 from E2, which acts as a priming event and converts the spike from the stable to metastable conformation (26, 27). At the plasma membrane, E2 interacts with the nucleocapsid core, and initiates budding and virus release. Particles may also bud from glycoprotein-containing vesicles called cytopathic vesicles II, and this pathway is used more by mosquito cells (28).

Voss et al. solved the Chikungunya virus (CHIKV) E2/E1 heterodimer in the metastable conformation and in complex with E3 at neutral pH in the stable conformation (29), and Li et al. solved the Sindbis virus (SINV) E2/E1 heterodimer at acidic pH (30). These structures showed the intra-dimer contacts within a heterodimer. Both groups fit the atomic heterodimers into cryo-EM structures of alphavirus virions to identify inter-dimer interactions, or contacts between heterodimers within the spike, and

between the E2 and nucleocapsid core. E1 consists of three domains: I-III. Domain II contains the fusion peptide and makes extended contacts with E2 in the intra-dimer heterodimer (29-31). This intra-dimer interface contains the acid-sensitive region and has been studied in regard to fusion regulation and mutations that expand vector range (32, 33). E2 has three domains: A-C. Domain B is the distal most domain and acts as a cap of the distal end of E1 protecting the fusion peptide (29, 30). In the low pH structure by Li et al., Domain B was disordered suggesting it is the first portion of the heterodimer to undergo conformational changes is response to low pH (30). Domain A in E2 is the central domain and Domain C is the closest to the lipid bilayer. Domain C is sandwiched between Domain II of E1 from its intra-dimer heterodimer and the Domain II of E1 from the adjacent heterodimer, or E1'. Both Voss et al. and Li et al. identified residues in E2 Domain C that contact residues in Domain II of E1' (29, 30). The inter-dimer contacts could have roles in both entry and assembly. Disrupting the inter-dimer contacts between E2 and E1' could affect trimer formation.

We hypothesized that E2 Domain C plays a key role in spike assembly. To test this hypothesis, we substituted six amino acids in SINV E2 Domain C to the corresponding residues in CHIKV, an alphavirus in a different clade (2, 34). The E2 residues that were mutated are predicted to interact with E1' residues in the adjacent dimer, or to "piggyback" on the dimers within a spike, and hence our mutant was named Chikungunya Piggyback (CPB). We determined CPB had slower growth and smaller plaques when grown in mammalian cells but not mosquito cells. CPB quickly gained second-site revertants, E2-H333N and E1-S247L, which were each able to restore growth in CPB. CPB grown in mammalian cells form particles with assembly defects but

the revertants restored their assembly to various degrees. Further analysis of the spike conformations on the CPB by cryo-EM showed the spikes in CPB were more flexible than the spikes in WT virus.

RESULTS

Domain C of E2 important for spike trimerization

The atomic structure of the CHIKV E2/E1 heterodimer identified the interface between E2 and E1 within a heterodimer and the intra-dimer contacts that were present. When these heterodimers were placed into the cryo-EM density of intact SINV virions, the potential contacts between heterodimers, or inter-dimer contacts, were identified (Figure 1A-1C). In the virion, Domain C of the E2 protein was sandwiched between two E1 proteins, one in the same heterodimer and one from the adjacent heterodimer (Figure 1D, 1E) (29). We hypothesized that Domain C would be important for spike trimerization because these inter-dimer contacts would bridge or connect the individual E2-E1 dimers into trimers.

Voss et al, identified ten residues in E2 Domain C that contact 12 residues in E1 Domain II in the adjacent heterodimer (designated as E1') (29). In the low pH SINV E2/E1 heterodimer structure, Li et al identified three residues in E2 Domain C that contact four residues in E1′ Domain II, all also identified in the CHIKV structure (30). Residues E2-272 to E2-288 in Domain C contained a majority of the E2 inter-dimer contacts (Figure 1F, 1G). Using SINV as our parental virus, we mutated six residues in this region from SINV to residues found in CHIKV, which belongs to a different clade than SINV (Figure 1F, 1G) (2, 34). The resulting mutant was named CHIK-Piggy-Back

(CPB), as the SINV E1' residues "piggyback" on the six E2 residues that were introduced from CHIKV. We opted to focus on the E2 inter-dimer residues because there are fewer contact residues in E2 than E1 and we speculated that mutating a larger number of residues in E1 would have increased the chance of misfolding due to too many disrupted interactions within the E1 protein itself (21).

Growth of CPB is attenuated in mammalian cells but not mosquito cells

To determine the effect of our CPB mutation, we infected mammalian (BHK-21) and mosquito (C6/36) cells at an MOI of 1 and quantified infectious virus release over time. In BHK cells, the CPB growth was attenuated, producing virus 1 to 1.5 logs lower titer than WT SINV (Figure 2A) as early as 8 hours post-infection. Additionally, CPB had a mean plaque size of 1 mm compared to the mean plaque size of 2 mm for WT SINV (Figure 3A, 3C). In C6/36 cells, however, CPB grew at a similar rate compared to WT SINV (Figure 2B). When plaque assays were conducted in C6/36 cells, the observed plaque sizes were similar between CPB and WT SINV. BHK cells are typically grown at 37°C, while C6/36 cells are grown at 28°C. To rule out temperature dependence on growth, we also measured WT SINV and CPB growth in BHK cells grown at 28°C. We found that there was still a 1 to 1.5 log reduction in CPB titer relative to WT SINV (Figure 2C) suggesting attenuated CPB growth is an effect of different host cells rather than different temperatures.

Two separate second-site revertants identified for CPB

As we worked with the CPB virus, we noticed that the virus reverted quickly as indicated by the change in plaque size phenotype from small to large. Changes in plaque size were evident often after cells were infected more than 40 hours or passaged more than two or three times (Figure 3A). To isolate revertants, we passaged CPB in BHK cells and saw a mixed plaque phenotype. We isolated and plaque-purified larger plaques, and then isolated and sequenced the viral RNA. We identified two independent single-site revertants, E2-H333N and E1-S247L (Figure 3B). E2-H333N was seen four times, and E1-S247L was seen once. Another mutation, E1-P250S, was seen twice but only in combination with E2-H333N. We focused on E2-H333N and E1-S247L since these single-sites potentially changed the virus fitness on their own. Both the E2-H333N and E1-S247L mutations were in close proximity to the inter-dimer interface (Figure 3B). E2-H333N is spatially near the six-residue cluster we mutated in E2, approximately 13 Å away from the center of the E2 inter-dimer contacts. E1-S247L is approximately 20 Å away from the center of the ten residues of E1' which interact with the six residues of E2. SINV E1 is glycosylated at position 245. The E1-S247L mutation abrogates the N-X-S/T motif needed for N-linked glycosylation at residue E1 245 (35), by changing the Ser at position 247 to Leu (Table 1).

To determine how these point mutations affect viral assembly, both of these mutations were inserted back into CPB and the WT SINV virus. The plaque sizes of the two revertants cloned into CPB were larger, comparable to that seen with WT SINV virus. The mean plaque size of CPB E2-H333N was 1.6 mm and of CPB E1-S247L was 1.9 mm; both larger than CPB which was 1 mm (Figure 3C). Next, growth kinetics of CPB E2-H333N and CPB E1-S247L were examined independently by infecting BHK

cells (Figure 3D). Both revertants resulted in a higher virus yield which grew between 1-2 logs better than the parental CPB and at a similar rate as WT SINV, indicating that both revertants rescued growth in CPB background. We also conducted growth kinetics in C6/36 cells (Figure 3E) and observed no difference between the two revertants in CPB, CPB and WT SINV. When the two mutations were independently cloned into the WT SINV backbone and the viral growth examined in both BHK and C6/36 cells, we observed no change in plaque size or growth kinetics. These results indicate that both of the mutations are neither deleterious nor enhancing in the absence of the CPB mutations.

CPB particles show defects in spike incorporation compared to WT SINV

Alphavirus spikes initially form dimers and then these dimers trimerize before localizing to the plasma membrane. If the spikes do not trimerize, transport to the plasma membrane is reduced. Spike trimerization is thought to be important for alphavirus budding. In our CPB mutant, we used the alphavirus structures and targeted residues that we thought would disrupt spike trimerization but not dimerization. To determine how particle budding was affected in the CPB mutant, we looked at the composition and morphology of purified virus particles from both BHK and C6/36 cells.

We purified virus particles through a sucrose cushion, ran them on an SDS-PAGE gel, and examined the protein composition. We noticed that BHK purified CPB particles have significantly reduced amounts of E1 and E2 glycoproteins relative to capsid protein when compared to the amounts of these proteins in WT SINV (Figure 4A). The E1 protein band in CPB E1-S247L migrates faster than E1 in WT SINV. The E1 protein in

CPB E1-S247L is at the same position as the E1 band in the SINV E1-N245/246Q virus which is known to have one of the two E1 glycosylation sites disrupted resulting in a faster migrating E1 protein band. As an additional control, the purified virion of SINV E1-N139Q/E2-N318Q which has one E1 glycosylation site and one E2 glycosylation site disrupted resulting in faster migration in both of those protein bands (Figure 4A) was also included (35).

In contrast to BHK cells, C6/36 purified CPB particles showed similar amounts of E1 and E2 glycoproteins to WT SINV (Figure 4B). The revertants also had similar protein composition to WT SINV with CPB E1-S247L having a faster migrating E1 protein band (Figure 4B). In both CPB and CPB E2-H333N virions, the E2 protein is a smeared band suggesting heterogenous glycosylation on the E2 protein (36).

CPB particles from mammalian cells show defects in particle morphology, which are partially or fully rescued by revertants

The reduced amount of glycoproteins in CPB particles suggested that the CPB particle may be morphologically different compared to WT particles. To test this, we stained our particles with uranyl acetate and imaged using transmission electron microscopy (TEM). WT SINV is approximately 70 nm in size and spherical and this is observed in both WT particles purified from BHK (Figure 4C) and C6/36 cells (Figure 4D). CPB, however, made almost no identifiable virus particles when purified from BHK cells (Figure 4C). We also noticed that any visible particles were not spherical. CPB E2-H333N partially rescued particle morphology while CPB E1-S247L fully recovered particle morphology (Figure 4C). CPB E2-H333N made more particles than CPB, and

some of them looked to be around 70 nm in size; however, many non-spherical particles were still seen. On the other hand, CPB E1-S247L made primarily spherical particles of 70 nm diameter, similar to WT SINV. In both CPB E2-H333N and CPB E1-S247L, there are also small particles ranging in size of approximately 10-40 nm, which could be assembly intermediates or disassembled fragments. These smaller particles suggest that CPB E2-H333N and CPB E1-S247L particles may still be fragile compared to WT SINV, despite being just as infectious.

WT SINV, CPB, and revertant virus particles purified from C6/36 were spherical and homogenous in shape, consistent with no major assembly or growth defects (Figure 4D). CPB particles appeared to have dimples or creases. This could suggest that even in C6/36 cells the mutations made in CPB are detrimental to proper spike formation or have defects in assembly but are still good enough that infectious particle assembly occurs (28).

Glycoprotein transport is not significantly affected in CPB

The low amounts of glycoproteins in CPB virions compared to WT SINV virions from BHK cells led us to two hypotheses. One, CPB has defects in spike trimerization and transport to the plasma membrane is diminished. Or second, CPB virions are misassembled because inter-dimer contacts have been disrupted. As a result, CPB may disassemble more than WT SINV during the purification process. These options are not mutually exclusive.

We used immunofluorescence to test if glycoprotein transport was altered in CPB compared to WT SINV. We infected BHK cells at an MOI of 2 for ten hours, a time

where there was a difference in infectious particles released and probed for glycoproteins at the cell membrane (Figure 5). Cells were fixed with paraformaldehyde, a non-permeabilizing fixative, and probed for SINV glycoproteins. Under these infection conditions, cells were not displaying CPE (Figure 5A, 5C). There was no drastic difference in glycoprotein levels at the plasma membrane between WT SINV, CPB, and revertant infected cells (Figure 5C, 5D). Virus-infected cells were equally healthy and had comparable amounts of detectable glycoproteins.

Spikes in CPB particles are distorted compared to WT SINV

The difference in particle morphology between CPB and WT SINV in mammalian cells was striking when imaged by TEM (Figure 4C, 4D). To further examine the particle structure and spike morphology, we purified virions and used cryo-EM to solve their 3D reconstructions. We focused on WT SINV, CPB, and the revertant CPB E1-S247L since these had the most extreme phenotypes and their structures would be most clear by cryo-EM (Figure 6). We imposed icosahedral averaging (Table 2) during the reconstruction process. The overall structural organizations of all six particles (WT SINV, CPB, CPB E1-S247L from BHK and C6/36) were preserved (Figure 6A-F). There are 80 petal-like spikes arranged into a T=4 surface lattice; the white triangle delineates one asymmetric unit (Figure 6A) (37). No clear E3 density was observed in any of the particles, consistent with what has been previously observed with SINV (8). The glycan modification at E2-196, located at the distal end of the E2 protein, was clearly seen when the estimated resolution is better than 10 Å (Figure 6G, GI, GL, red arrows). As seen in other alphavirus structures (7, 38-42), the E1 protein contributes to the

continuous shell underneath the spikes (Figure 6A-F, yellow color) with holes at every twofold and fivefold above the membrane.

However, when looking more carefully at the enlarged view of each spike at the quasi-threefold axis, (dotted circle Figure 6A) there were discernable differences. We chose the quasi three-fold spike because spikes at the 5-, 3-, 2- fold would, by default of icosahedral symmetry, be identical. The spikes at the quasi symmetry axes would not have any symmetry imposed on them and differences in morphology would be more evident. The irregular density at the inter-dimer location of the spike was clearest in CPB purified from BHK cells (Figure 6H, black arrows). Note that the density of two lobes at the spike petal were fused together, while the other heterodimer within the same spike remained separate (Figure 6B, BHK CPB). For the other five particles, the E1/E2 dimers within a spike were organized in a trimeric manner with no distinct breaks in the spikes.

DISCUSSION

To investigate the role of the inter-dimeric contacts in assembly, we used a structure-guided approach and mutated six residues in E2 that, in the stable and metastable structures of the spike, form one portion of an interface with the adjacent E1' protein. We called this mutant CPB. We found that CPB growth is attenuated in mammalian cells but not mosquito cells. In addition, CPB particle morphology is defective in mammalian cells, but minimally affected in mosquito cells. This work suggests that there is a host factor that is involved in the trimerization of E2-E1 heterodimers since the same viral proteins are assembling in each host cell. If this

assembly was autonomous, we would not observe a host-specific difference. The difference could be due to different post-translational modifications by the host, different host-protein chaperones affecting virus assembly, or a combination of both. BHK and C6/36 cells are defective in innate immune responses so the attenuation in growth is not a host response to infection.

Although our studies suggest that trimerization primarily affects assembly and not entry, it is difficult to separate assembly defects from downstream entry impacts. While we always infect cells with the same number of infectious particles per cell in our infections, CPB growth will quickly fall behind WT SINV because of its assembly defects.

The assembly pathway in CPB is defective

In mammalian cells, CPB glycoprotein levels are comparable to WT SINV in cell lysates, and glycoprotein expression on the cell surface is similar to WT SINV as well. However, CPB particles have fewer glycoproteins compared to WT SINV particles. Our cryo-EM models of CPB show that CPB particles do not have three symmetrical lobes. Figure 6 shows a visible gap between two of the lobes and the third, which could suggest that two heterodimers are interacting but the third is not. We conclude that CPB glycoproteins are being translated and maintained at the same levels as WT and are being transported to the plasma membrane. However, the defects in CPB are seen during budding or post purification. In particular, CPB does not result in particles with the same spike to capsid ratio as WT SINV. One hypothesis is that CPB glycoproteins are not properly assembling into spike trimers. Because optimal contacts between

heterodimers are not being made, these trimers may be more fragile and during our purification process the particles disassemble. Alternatively, the transmembrane domains and endodomain of E2 are ill-positioned and the minimal E2-CP contacts needed for budding are not present. Since the CPB trimer clearly has a different conformation than the WT SINV trimer, it could be that the tail of E2 is no longer able to interact with capsid in a 1:1 ratio. It also could be that these CPB particles have fewer than the typical 80 spikes. Since we do not know how many spikes are needed for an infection, there may still be enough spikes in CPB particles to be somewhat infectious. Interestingly, our TEM images show that CPB S247L produces particles that are much more WT-like than CPB H333N, despite both revertants restoring CPB growth. This suggests that a virus particle does not need to be perfectly shaped in order to be infectious.

Our immunofluorescence results show that glycoprotein transport to the plasma membrane is comparable between CPB and WT SINV. However, nothing about the conformation of the spikes can be concluded. Furthermore, while E2-E1 are most stable as heterodimers, small amounts of the monomeric proteins will localize to the plasma membrane (15). Our results cannot differentiate conformation or oligomeric state of the glycoproteins at the cell surface.

Possible implications of revertant residues

CPB quickly reverted resulting in two independently fit mutations, E2-H333N and E1-S247L, and one mutation, P250S, which was seen only in combination with E2 H333N. E2-H333N, E1-S247L, and P250S are all in close proximity to the cluster of mutations

made at the inter-dimer interface, although none were identified by Voss or Li as one of the inter- or intra-dimer contact residues (29, 30). Residue 333 for most viruses is either a histidine or an asparagine. Additionally, the corresponding residue for SINV H333 is N330 in CHIKV. Because the histidine side chain has a pKa of 6.00, it is within the range of different pH environments in the host cell. This histidine residue may affect CPB either during entry, specifically during disassembly in the endosome (43, 44), or during assembly as the E2-E1 heterodimer travels through the ER and Golgi (45). The role in disassembly could be unfavorable in CPB, since it may have a less stable trimer and less stable heterodimers even without a low pH environment. During assembly of the CPB E2-E1 heterodimers, there may be improper folding possibly making trimer assembly more sensitive to pH which cannot occur with H333.

S247L interferes with N-linked glycosylation motif that allows E1-N245 to be glycosylated. In CHIKV, there is only one glycosylation site on E1 at N141 versus two in SINV, one at N139 and one at N245 (Table 1) (35, 38). Although residue 247 is not conserved among alphaviruses, it is clear that some viruses including SINV have the N-X-S/T glycosylation motif at N245, while others including CHIKV do not. It is interesting that CPB S247L appears more WT-like in particle morphology than CPB H333N. It is possible that de-glycosylation at this site allows for better folding or removes a steric hinderance that allows for trimerization.

From our revertant sequencing we also saw that in some instances when E2-H333N was mutated, E1-P250S was also mutated. Residue 250 is a proline residue in SINV and a serine residue in CHIKV. It was seen with H333N but does not seem necessary for restoring growth since H333N was seen alone two times and CPB H333N

independently restored growth. However, the proline residue in CPB might disrupt folding since it is unable to form hydrogen bonds. This could explain why CPB H333N has less spherical looking particles, despite having growth comparable to that of WT SINV. In all three cases, it appears that CPB is reverting to be more like CHIKV.

Other revertants in spike proteins that show host specificity

Our work is not the first time a mutation has shown host specificity in alphaviruses. In CHIKV, Ashbrook et al., showed a mutation at E2 G82R enhanced infectivity in mammalian cells but reduced infectivity in mosquito cells and reduced virulence in mouse model (46). This residue is present on the exterior of the E2 protein and was determined to be important to GAG binding, entry and virulence.

Jupille et al. identified Ross River E2 Y18H as having a fitness advantage in mosquito cells and a disadvantage in mammalian cells (47). This residue lies in the intra-dimer interface of the E2-E1 heterodimer. Interestingly, in the Ross River clade, the viruses have either a tyrosine or a histidine at position 18 and the authors suggest, this residue serves as a regulator of fitness between the mosquito vector and mammalian host (47). In our work, the revertant E2 H333N was isolated. Most alphaviruses are either a histidine or asparagine at this residue emphasizing the structural and functional requirement of this residue.

Our work presented here is the first example of a mutation that has host specificity and mapping to defects in spike assembly. Further work needs to be done to dissect the exact mechanism of where in the spike assembly pathway the CPB mutant fails in mammalian cells and how the revertants overcome these defects. Presented results

now allow us to further identify host-specific chaperones and factors necessary for alphavirus glycoprotein folding and oligomerization and possibly extend to other arboviruses that assemble in multiple host environments.

Materials and Methods

Viruses and cells

The virus strains used in this work were the TE12 strain of SINV and 181/21 strain of CHIKV (a gift from Dr. Terrence Dermody). BHK-21 cells (BHK) (American Type Culture Collection, Manassas, VA) were grown in minimal essential medium (Mediatech, Manassas, VA) supplemented with 10% fetal bovine serum (FBS; Atlanta Biologicals, Lawrenceville, GA), nonessential amino acids, L-glutamine, and antibiotic-antimycotic solution (Corning, Corning, NY). BHK-21 cells were grown at 37°C in the presence of 5% CO_2, or at 28°C in the presence of 5% CO_2. C6/36 cells (American Type Culture Collection, Manassas, VA) were grown in identical medium at 28°C in the presence of 5% CO_2.

Generation of wild-type and mutant viruses

The CPB mutant virus was generated using a two part QuikChange site-directed mutagenesis (Agilent, Santa Clara, CA) of the TE12 SINV cDNA clone. First the residues between nucleotides 9444 and 9494 were deleted, and then the chimera sequence was inserted. No additional changes were introduced to the chimera virus during cloning. The mutations were confirmed by sequencing the E2 region. The CPB

E2-H333N and CPB E1-S247L were generated by QuikChange site-directed mutagenesis.

Wild-type and mutant cDNA clones were linearized with Sac I and in vitro transcribed with SP6 polymerase at 39°C for 2 hr. For electroporation of BHK cells, approximately 10^7 BHK cells were trypsinized, washed two times with phosphate-buffered saline (PBS), and resuspended with PBS to a final volume of 500 µl. The cells were mixed with *in vitro*-transcribed RNA in a 2-mm-gap cuvette and pulsed once at 1.5 kV, 25 µF, and 200 Ω using a Bio-Rad Gene Pulser Xcell electroporation system (Bio-Rad Laboratories, Hercules, CA). Following a 5-min recovery at room temperature, the cells were diluted 1:10 in cell medium and incubated at 37°C in the presence of 5% CO_2. At the indicated time points (around 24 hours post infection for WT, CPB E2-H333N, CPB E1-S247L, and 40 hours post infection for CPB), virus was harvested, and the titer was determined using a standard plaque assay procedure (23). Plaques were detected at 48 hours post-infection by formaldehyde fixation and crystal violet staining.

One-step growth analysis

Confluent 12-well plates of BHK cells were infected with virus at MOI of 1 at room temperature for 1 hr. Following this adsorption period, the cells were washed with PBS to remove any unbound particles, and 400 µL of media was added. At the indicated time points, 400 µL media was removed and replaced with fresh media. The titers of these samples were determined by standard plaque assay and plotted against time.

Identification of second-site revertants

Large plaques were detected from media of CPB infected BHK cells more than 40 hours post-electroporation. As previously described (23), large plaques were isolated and used to infect BHK cells. The infected cells were lysed at 14 hours post-infection with TRIzol reagent (Invitrogen, Carlsbad, CA), and cytoplasmic RNA was isolated using chloroform extraction. The coding sequence of the structural polyprotein was amplified from the viral RNA using RT-PCR and two primers, one specific for the E1 region and the other specific for the E2 region. The region corresponding to the structural polyprotein was sequenced to identify the location of the potential second-site mutation. To verify that the large plaque phenotypes were due to the mutation identified in sequencing, the revertant sites were introduced back into the chimeric viruses and growth kinetics and plaque sizes were analyzed.

Virus purification

150 mm dishes were infected with 3 mL virus at a MOI of 0.1 at room temperature for 1 hr. After the adsorption period, the cells were overlaid with 15 mL serum-free media (Thermo Fisher Scientific life technologies, Waltham, MA) supplemented with nonessential amino acids, L-glutamine, and antibiotic-antimycotic solution (Corning). Medium was collected approximately 24 hours post infection for BHK cells. For C6/36 cells, 5 mL fresh serum-free media was added after 72 hours, and medium was collected after approximately 120 hours post infection. The medium was then spun down at 1157 × g for 5 min at 15°C to remove cells and cell debris. Virus particles from the clarified medium was pelleted through sucrose cushion. The clarified medium was

overlaid onto 3 ml 27% sucrose in 20 mM HN buffer (20 mM HEPES, pH 7.5, and 150 mM NaCl) and spun at 140,000 × g for 2.5 h at 15°C (36, 48).

SDS PAGE gel of purified virus particles

Purified virus particles were loaded onto an 8% SDS gel containing 0.5% 2,2,2-trichloroethylene v/v in the resolving gel, and run for approximately 45 minutes at 200 V. The gel was imaged with the Bio-Rad ChemiDoc MP Imaging System using the stain-free image setting. The PageRuler prestained protein ladder (Thermo Fisher Scientific-Invitrogen, Waltham, MA) was used in all studies.

Immunofluorescence analysis of cell surface spike protein expression

The primary antibodies recognizing SINV glycoproteins were pre-cleared to reduce background signal from non-specific cell binding. A confluent well of BHK cells was washed twice with PBS, chilled with PBS for 2 hours, and then incubated at 4°C with 200 µL of a 1:10 dilution of antibody in cold PBS for 2 hours while rocking. The antibody mixture was removed and centrifuged, and the supernatant was saved and used in immunofluorescence studies.

BHK cells were grown on coverslips and at approximately 75% confluency were infected with virus at an MOI of 2 at room temperature for 90 minutes. After this adsorption period, fresh media was added, and cells were incubated at 37°C in the presence of 5% CO_2. Ten hours post infection, the cells were washed with PBS and then fixed with 4% paraformaldehyde (Thermo Fisher Scientific Life Technologies, Waltham, MA) at room temperature for 10 minutes. 16% EM-grade paraformaldehyde

was diluted in PBS to make 4% paraformaldehyde; the EM-grade paraformaldehyde is methanol-free to avoid permeabilization. The cells were then washed, blocked in 2.5% BSA in PBS for 30 minutes, and incubated with pre-cleared polyclonal anti-E2/E1 (1:50 of pre-cleared) in 2.5% BSA for 45 minutes. Cells were washed and incubated with Alexa 488 Goat anti-Rabbit secondary antibody (1:5000) in 2.5% BSA in PBS for 45 minutes in the dark. Cells were then washed and stained with DAPI. The coverslips were carefully removed, dipped in distilled water and blotted, and inverted onto 5 µL of Aqua-Poly/Mount (Polysciences, Warrington, PA) on a slide. Slides were imaged using an Olympus 1X71 fluorescence microscope (Olympus, Center Valley, PA).

Transmission electron microscopy

Four µL of purified virus was applied to a Formvar- and carbon-coated 400-mesh copper grid (Electron Microscopy Sciences, Hatfield, PA) for 25 seconds, washed with 4 µL water for 25 seconds, and stained with 2% uranyl acetate for 25 seconds. The stained grids were analyzed using a JEOL 1010 transmission electron microscope (Tokyo, Japan) operating at 80 kV. Images were recorded using a Gatan UltraScan 4000 charge-coupled-device camera (Pleasanton, CA).

Cryo-EM imaging and 3D reconstruction

To prepare a frozen-hydrated cryo-EM specimen, approximately 4 µL of purified virus sample was applied to a glow-discharged 300-mesh copper grid coated with continuous carbon film (Electron Microscopy Sciences, Hatfield, PA). The grid was plunged into a liquid ethane container that is further cooled by a liquid nitrogen bath. This process was performed using Vitrobot Mark IV under 4 degree and 100% humidity

(Thermo Fisher Scientific-Invitrogen, Waltham, MA). Frozen-hydrated cryo-EM grids for all samples except SINV WT (C6/36) were clipped into cartridges and then transferred into a cassette according to the manufacture protocol. The cassette was loading inside a 300-kV Titan Krios G3i equipped with Gatan BioContinuum™ K3 direct electron detection camera. Data acquisition was set up using TFS EPU under counted super-resolution mode. The nominal magnification is 64,000x (equal to 0.7 Å per pixel) and the illumination has a dose rate of 1 $e^-/Å^2$ per frame under the exposure preset with a total dose of 30 $e^-/Å^2$. Zero-loss peak was aligned every hour with an energy slit opened at 20 eV. Data collection for SINV WT (C6/36) was done by using a 300-kV JEOL JEM-3200FS TEM equipped with DE-12 CMOS camera (Direct Electron). The frozen hydrated grid was transferred to a Gatan 626 cryo-holder and inserted into the TEM. The nominal magnification was set to 80,000x (equal to 1.9 $e^-/Å^2$). The zero-loss peak was aligned at the beginning of the data collection with a slit opened at 20 eV. The total accumulated dose is ~30 $e^-/Å^2$.

Image analysis was performed using Relion (v3.1) (49). Initial particle picking was done by Laplacian-of-Gaussian filtered auto-picking method implemented in Relion (50). Subsequently, 2D classification was used to eliminate the noise density that got picked earlier and the 3D initial model was built de novo. This initial model was then used as a template for automatic particle picking for all samples. Similarly, multiple runs of 2D classification and 3D refinement were performed to obtain the final 3D models (summarized in Table 2). Each volume was rendered using UCSF ChimeraX (51).

Acknowledgements

We thank IU Virology group for constructive discussions and Jim Powers, Walczak and Shaw labs for help with microscopy. Funding for this work from IU Wells Scholars Program and LS McClung Fellowship (SCR), the startup fund from The Pennsylvania State University College of Medicine to J.C.-Y.W and IU IAS (SM). We also gratefully acknowledge The Pennsylvania State University College of Medicine for access to the Cryo-EM (RRID:SCR_021178) and the HPC core facilities.

FIGURE LEGENDS

Figure 1: Inter-dimer interface residues in Domain C of E2 may be important for spike assembly. (A) Crystal structure of CHIKV glycoproteins E2 (blue) and E1 (yellow) (PDB ID: 3N40) (29) fit into cryo-EM map of SINV (PDB ID:1Z8Y) (30). One trimeric spike is outlined. (B) During assembly, E1 (*shades of yellow*) forms heterodimers with E2 (*shades of blue*), and these dimers then trimerize. A top view of one of these trimeric spikes, with the individual E2 (in teal, light blue, and blue) and E1 (in gold, light yellow, and saffron) proteins is shown here. A total of 80 spikes are on the surface of the alphavirus particle. (C) The trimer is rotated 90 degrees for a side view. The light blue E2 and light yellow E1 are a heterodimer. Intra-dimer contacts occur between Domains I and II of E1 with Domains A, B, C of E2. The teal E2’ and gold E1’ form another heterodimer, with similar intra-dimer contacts. The last dimer in the spike is shown in grey. (D) A 60-degree rotation of (C) highlights an inter-dimer interface in the trimer. Inter-dimer contacts are between the gold E1’ of one heterodimer and the light blue E2 in the adjacent dimer. Domain C of E2 (red dashed circle) is sandwiched between the adjacent E1’ (gold) and its cognate E1 (light yellow), forming inter-dimer and intra-dimer

contacts respectively. (E) The inter-dimer between E1' and E2 are shown. (F) Ribbon diagram of the inter-dimer highlighting a 6-residue cluster of E2 *(blue spheres)* within Domain C that has been identified to make inter-dimer contacts with ~10 unique residues of E1' *(yellow spheres).* The blue residues were mutated in this study. (G) Amino acid alignment of CHIKV and SINV E2 in the inter-dimer region; SINV residues shown in black and CHIKV residues shown in red. The CHIK-Piggy-Back (CPB) chimera was generated by substituting the non-homologous E2 CHIKV residues for the corresponding SINV E2 residues (*highlighted in red in CPB)* in this region.

Figure 2: CPB grows slower than WT SINV in mammalian cells, but not mosquito cells. Cells were infected at an MOI of 1. At the indicated time points, media was collected and replaced with fresh media. The titers of the collected samples were determined by standard plaque assay on BHK cells. Results are shown for one representative experiment (N=5). (A) Growth kinetics of infectious virus released from BHK cells at 37°C show CPB was attenuated by 1-1.5 logs relative to WT SINV. (B) Growth kinetics of virus grown in C6/36 cells at 28°C show CPB releases infectious particles at the same rate as WT SINV. (C) Growth kinetics of virus grown in BHK cells at 28°C show that CPB growth is still attenuated by 1-1.5 logs relative to WT SINV.

Figure 3: Two CPB revertants map close to the inter-dimer interface and grow similarly to WT SINV. (A) CPB collected 20-40 hours post-electroporation have smaller plaques compared to WT SINV plaques. When CPB is harvested later, or as it is passaged in BHK cells, larger plaques are seen in addition to the small plaques. Five of

these larger plaques were isolated, the RNA was sequenced, and two independent second-site revertants were found. (B) The locations of two second-site revertant sites, H333N in E2 (*cyan*) and S247L in E1 (*red)*, are shown relative to the inter-dimer contacts identified in Figure 1F. (C) CPB E2-H333N and CPB E1-S247L were introduced independently into CPB. Plaque size of CPB E2-H333N and CPB E1-S247L in BHK cells was larger compared to CPB. (D) Growth kinetics of the two revertants show they have comparable titers as WT SINV in BHK and (E) C6/36 cells. Representative curves are shown (N=3). Cells were infected at an MOI of 1, media was collected at the indicated time points, and samples titered on BHK cells.

Figure 4: Particle morphology and composition is restored in CPB revertants to varying degrees. Cells were infected at a MOI of 0.1 for 1 hour, after which serum-free media was overlayed. Infected BHK media was collected after 24 hours, and infected C6/36 media was collected after 120 hours. The media was clarified and purified through a sucrose cushion at 140,000 × g for 2.5 h. (A and B) To determine the composition of the virions, purified virus was solubilized in reducing SDS sample buffer, run on an 8% SDS-PAGE gel, and imaged by stain-free TCE. CPB particles have a reduced levels of E2/E1 glycoproteins in particles purified from BHK cells. The E1 deglycosylation control is SINV E1-N245/246Q, which has one of its two E1 glycosylation sites deglycosylated resulting in a faster migrating E1 protein band, and the E1/E2 deglycosylation control is E1-N139Q/E2-N318Q and has a deglycosylation site in both E1 and E2 resulting in faster migration in each of those protein bands. (C and D) Purified particles were applied to a Formvar- and carbon-coated 400-mesh

copper grid, stained with 2% uranyl acetate, and imaged at ×20,000 magnification with the JEOL 1010 transmission electron microscope. Scale bar for TEM = 200nm.

Figure 5: CPB glycoprotein spikes are transported to the plasma membrane of BHK cells in approximately equal amounts compared to WT. BHK cells were infected at an MOI of 2. Ten hours post-infection, the cells were fixed with 4% EM-grade paraformaldehyde and probed for SINV E1/E2. Images were taken at ×40 magnification on a Nikon Ni-E microscope. Representative images are shown (N=4). (A) Brightfield images and (B) DAPI staining show cells in field of view and their nuclei in blue. (C) Cell surface E2/E1 expression shown in green, Alexa Fluor 488 was the secondary antibody. (D) Anti-E2/E1+DAPI merge shows green fluorescence from surface glycoprotein expression relative to the cells present.

Figure 6. Cryo-EM 3D reconstructions show that CPB spikes from mammalians cells have an altered interdimer organization. (A-F) Radially colored isosurface rendering of WT SINV, CPB, and SINV E1-S247L from BHK cells (A-C, top row) and C6/36 cells (D-F, bottom row). All views are at the 5-fold axis. All six maps have a similar outer appearance with 80 spikes decorating a fenestrated surface. In (A), the white triangle shows one asymmetric unit. Filled oval, triangle, and pentagon indicate locations of twofold, threefold and fivefold axes, respectively. The dotted circle shows one of the spikes on the quasi-three axis. (G-L) Enlarged views of SINV spikes at the quasi-threefold location. The spike of CPB from BHK (H) shows a distinct organization from other SINV spikes. Black arrowheads indicate the difference in the electron density between each interdimer interface. Red arrowheads show glycan modification at E2-196.

REFERENCES

1. Griffin DE. 2013. Chapter 23: Alphaviruses, p 652-770. *In* Knipe DM, Howley PM (ed), Fields' Virology. Lippincott Williams & Wilkins, Philadelphia, PA.

2. Kuhn RJ. 2013. Chapter 22: Togaviradae, p 629-650. *In* Knipe DM, Howley PM (ed), Fields' Virology. Lippincott Williams & Wilkins, Philadelphia.

3. Hermanns K, Marklewitz M, Zirkel F, Overheul GJ, Page RA, Loaiza JR, Drosten C, van Rij RP, Junglen S. 2020. Agua Salud alphavirus defines a novel lineage of insect-specific alphaviruses discovered in the New World. J Gen Virol 101:96-104.

4. Forrester NL, Palacios G, Tesh RB, Savji N, Guzman H, Sherman M, Weaver SC, Lipkin WI. 2012. Genome-scale phylogeny of the alphavirus genus suggests a marine origin. J Virol 86:2729-38.

5. Firth AE, Chung BY, Fleeton MN, Atkins JF. 2008. Discovery of frameshifting in Alphavirus 6K resolves a 20-year enigma. Virol J 5:108.

6. Chen R, Mukhopadhyay S, Merits A, Bolling B, Nasar F, Coffey LL, Powers A, Weaver SC, Ictv Report C. 2018. ICTV Virus Taxonomy Profile: Togaviridae. J Gen Virol 99:761-762.

7. Cheng RH, Kuhn RJ, Olson NH, Rossmann MG, Choi HK, Smith TJ, Baker TS. 1995. Nucleocapsid and glycoprotein organization in an enveloped virus. Cell 80:621-30.

8. Tang J, Jose J, Chipman P, Zhang W, Kuhn RJ, Baker TS. 2011. Molecular links between the E2 envelope glycoprotein and nucleocapsid core in Sindbis virus. J Mol Biol 414:442-59.

9. Jose J, Przybyla L, Edwards TJ, Perera R, Burgner JW, 2nd, Kuhn RJ. 2012. Interactions of the cytoplasmic domain of Sindbis virus E2 with nucleocapsid cores promote alphavirus budding. J Virol 86:2585-99.

10. Lee S, Owen KE, Choi HK, Lee H, Lu G, Wengler G, Brown DT, Rossmann MG, Kuhn RJ. 1996. Identification of a protein binding site on the surface of the alphavirus nucleocapsid and its implication in virus assembly. Structure 4:531-41.

11. Skoging U, Vihinen M, Nilsson L, Liljestrom P. 1996. Aromatic interactions define the binding of the alphavirus spike to its nucleocapsid. Structure 4:519-29.

12. Zhao H, Lindqvist B, Garoff H, von Bonsdorff CH, Liljestrom P. 1994. A tyrosine-based motif in the cytoplasmic domain of the alphavirus envelope protein is essential for budding. EMBO J 13:4204-11.

13. Melancon P, Garoff H. 1987. Processing of the Semliki Forest virus structural polyprotein: role of the capsid protease. J Virol 61:1301-9.

14. Mayne JT, Rice CM, Strauss EG, Hunkapiller MW, Strauss JH. 1984. Biochemical studies of the maturation of the small Sindbis virus glycoprotein E3. Virology 134:338-57.

15. Lobigs M, Zhao HX, Garoff H. 1990. Function of Semliki Forest virus E3 peptide in virus assembly: replacement of E3 with an artificial signal peptide abolishes spike heterodimerization and surface expression of E1. J Virol 64:4346-55.

16. Liu N, Brown DT. 1993. Transient translocation of the cytoplasmic (endo) domain of a type I membrane glycoprotein into cellular membranes. J Cell Biol 120:877-83.

17. Harrington HR, Zimmer MH, Chamness LM, Nash V, Penn WD, Miller TF, 3rd, Mukhopadhyay S, Schlebach JP. 2020. Cotranslational folding stimulates programmed ribosomal frameshifting in the alphavirus structural polyprotein. J Biol Chem 295:6798-6808.

18. Mulvey M, Brown DT. 1996. Assembly of the Sindbis virus spike protein complex. Virology 219:125-32.

19. Molinari M, Helenius A. 1999. Glycoproteins form mixed disulphides with oxidoreductases during folding in living cells. Nature 402:90-3.

20. Molinari M, Helenius A. 2000. Chaperone selection during glycoprotein translocation into the endoplasmic reticulum. Science 288:331-3.

21. Mulvey M, Brown DT. 1994. Formation and rearrangement of disulfide bonds during maturation of the Sindbis virus E1 glycoprotein. J Virol 68:805-12.

22. Mulvey M, Brown DT. 1995. Involvement of the molecular chaperone BiP in maturation of Sindbis virus envelope glycoproteins. J Virol 69:1621-7.

23. Snyder AJ, Mukhopadhyay S. 2012. The alphavirus E3 glycoprotein functions in a clade-specific manner. J Virol 86:13609-20.

24. Uchime O, Fields W, Kielian M. 2013. The role of E3 in pH protection during alphavirus assembly and exit. J Virol 87:10255-62.

25. Sjoberg M, Lindqvist B, Garoff H. 2011. Activation of the alphavirus spike protein is suppressed by bound E3. J Virol 85:5644-50.

26. Lobigs M, Garoff H. 1990. Fusion function of the Semliki Forest virus spike is activated by proteolytic cleavage of the envelope glycoprotein precursor p62. J Virol 64:1233-40.

27. Zhang X, Fugere M, Day R, Kielian M. 2003. Furin processing and proteolytic activation of Semliki Forest virus. J Virol 77:2981-9.

28. Jose J, Taylor AB, Kuhn RJ. 2017. Spatial and Temporal Analysis of Alphavirus Replication and Assembly in Mammalian and Mosquito Cells. MBio 8.

29. Voss JE, Vaney MC, Duquerroy S, Vonrhein C, Girard-Blanc C, Crublet E, Thompson A, Bricogne G, Rey FA. 2010. Glycoprotein organization of Chikungunya virus particles revealed by X-ray crystallography. Nature 468:709-12.

30. Li L, Jose J, Xiang Y, Kuhn RJ, Rossmann MG. 2010. Structural changes of envelope proteins during alphavirus fusion. Nature 468:705-8.

31. Lescar J, Roussel A, Wien MW, Navaza J, Fuller SD, Wengler G, Rey FA. 2001. The fusion glycoprotein shell of Semliki Forest virus: an icosahedral assembly primed for fusogenic activation at endosomal pH. Cell 105:137-48.

32. Tsetsarkin KA, Chen R, Leal G, Forrester N, Higgs S, Huang J, Weaver SC. 2011. Chikungunya virus emergence is constrained in Asia by lineage-specific adaptive landscapes. Proc Natl Acad Sci U S A 108:7872-7.

33. Tsetsarkin KA, Chen R, Yun R, Rossi SL, Plante KS, Guerbois M, Forrester N, Perng GC, Sreekumar E, Leal G, Huang J, Mukhopadhyay S, Weaver SC. 2014. Multi-peaked adaptive landscape for chikungunya virus evolution predicts continued fitness optimization in Aedes albopictus mosquitoes. Nat Commun 5:4084.

34. Weaver SC, Winegar R, Manger ID, Forrester NL. 2012. Alphaviruses: population genetics and determinants of emergence. Antiviral Res 94:242-57.

35. Pletnev SV, Zhang W, Mukhopadhyay S, Fisher BR, Hernandez R, Brown DT, Baker TS, Rossmann MG, Kuhn RJ. 2001. Locations of carbohydrate sites on alphavirus glycoproteins show that E1 forms an icosahedral scaffold. Cell 105:127-136.

36. Dunbar CA, Rayaprolu V, Wang JC, Brown CJ, Leishman E, Jones-Burrage S, Trinidad JC, Bradshaw HB, Clemmer DE, Mukhopadhyay S, Jarrold MF. 2019. Dissecting the Components of Sindbis Virus from Arthropod and Vertebrate Hosts: Implications for Infectivity Differences. ACS Infect Dis 5:892-902.

37. Zandi R, Reguera D, Bruinsma RF, Gelbart WM, Rudnick J. 2004. Origin of icosahedral symmetry in viruses. Proc Natl Acad Sci U S A 101:15556-60.

38. Basore K, Kim AS, Nelson CA, Zhang R, Smith BK, Uranga C, Vang L, Cheng M, Gross ML, Smith J, Diamond MS, Fremont DH. 2019. Cryo-EM Structure of Chikungunya Virus in Complex with the Mxra8 Receptor. Cell 177:1725-1737 e16.

39. Hasan SS, Sun C, Kim AS, Watanabe Y, Chen CL, Klose T, Buda G, Crispin M, Diamond MS, Klimstra WB, Rossmann MG. 2018. Cryo-EM Structures of Eastern Equine Encephalitis Virus Reveal Mechanisms of Virus Disassembly and Antibody Neutralization. Cell Rep 25:3136-3147 e5.

40. Kostyuchenko VA, Jakana J, Liu X, Haddow AD, Aung M, Weaver SC, Chiu W, Lok SM. 2011. The structure of barmah forest virus as revealed by cryo-electron microscopy at a 6-angstrom resolution has detailed transmembrane protein architecture and interactions. J Virol 85:9327-33.

41. Ribeiro-Filho HV, Coimbra LD, Cassago A, Rocha RPF, Guerra J, de Felicio R, Carnieli CM, Leme L, Padilha AC, Paes Leme AF, Trivella DBB, Portugal RV, Lopes-de-Oliveira PS, Marques RE. 2021. Cryo-EM structure of the mature and infective Mayaro virus at 4.4 A resolution reveals features of arthritogenic alphaviruses. Nat Commun 12:3038.

42. Chen L, Wang M, Zhu D, Sun Z, Ma J, Wang J, Kong L, Wang S, Liu Z, Wei L, He Y, Wang J, Zhang X. 2018. Implication for alphavirus host-cell entry and assembly indicated by a 3.5A resolution cryo-EM structure. Nat Commun 9:5326.

43. White J, Kielian M, Helenius A. 1983. Membrane fusion proteins of enveloped animal viruses. Q Rev Biophys 16:151-95.

44. White J, Helenius A. 1980. pH-dependent fusion between the Semliki Forest virus membrane and liposomes. Proc Natl Acad Sci U S A 77:3273-7.

45. Paroutis P, Touret N, Grinstein S. 2004. The pH of the secretory pathway: measurement, determinants, and regulation. Physiology (Bethesda) 19:207-15.

46. Ashbrook AW, Burrack KS, Silva LA, Montgomery SA, Heise MT, Morrison TE, Dermody TS. 2014. Residue 82 of the Chikungunya virus E2 attachment protein modulates viral dissemination and arthritis in mice. J Virol 88:12180-92.

47. Jupille HJ, Medina-Rivera M, Hawman DW, Oko L, Morrison TE. 2013. A tyrosine-to-histidine switch at position 18 of the Ross River virus E2 glycoprotein is a determinant of virus fitness in disparate hosts. J Virol 87:5970-84.

48. Wang JC, Mukhopadhyay S, Zlotnick A. 2018. Geometric Defects and Icosahedral Viruses. Viruses 10.

49. Scheres SH. 2016. Processing of Structurally Heterogeneous Cryo-EM Data in RELION. Methods Enzymol 579:125-57.

50. Zivanov J, Nakane T, Forsberg BO, Kimanius D, Hagen WJ, Lindahl E, Scheres SH. 2018. New tools for automated high-resolution cryo-EM structure determination in RELION-3. Elife 7.

51. Pettersen EF, Goddard TD, Huang CC, Meng EC, Couch GS, Croll TI, Morris JH, Ferrin TE. 2021. UCSF ChimeraX: Structure visualization for researchers, educators, and developers. Protein Sci 30:70-82.

Fig 1

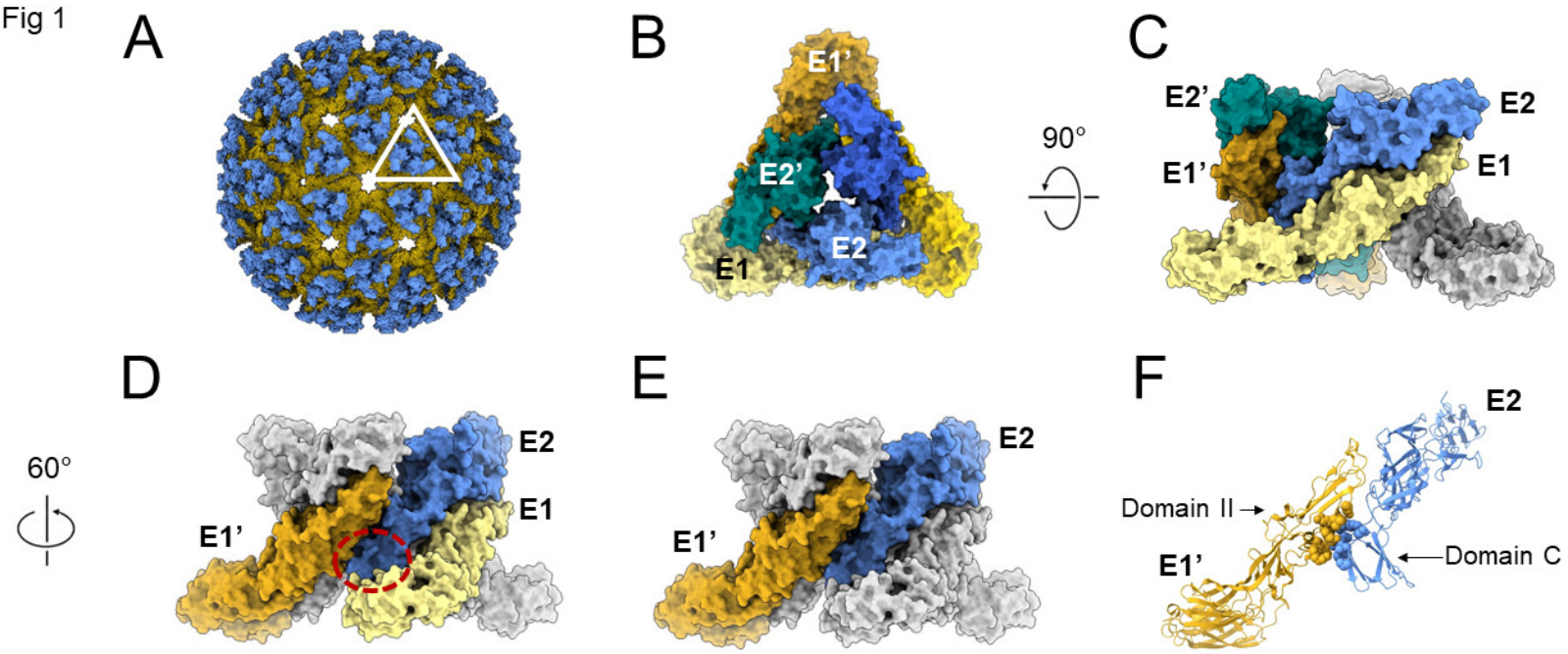

G

SINV	E2:	272	H	A	P	N	V	I	H	G	F	K	H	I	S	L	Q	L	D	288
CPB	E2:	272	R	N	P	T	V	T	H	G	F	K	H	I	S	L	L	L	Y	288
CHIKV	E2:	272	R	N	P	T	V	T	Y	G	K	N	Q	V	I	M	L	L	Y	288

Fig 2

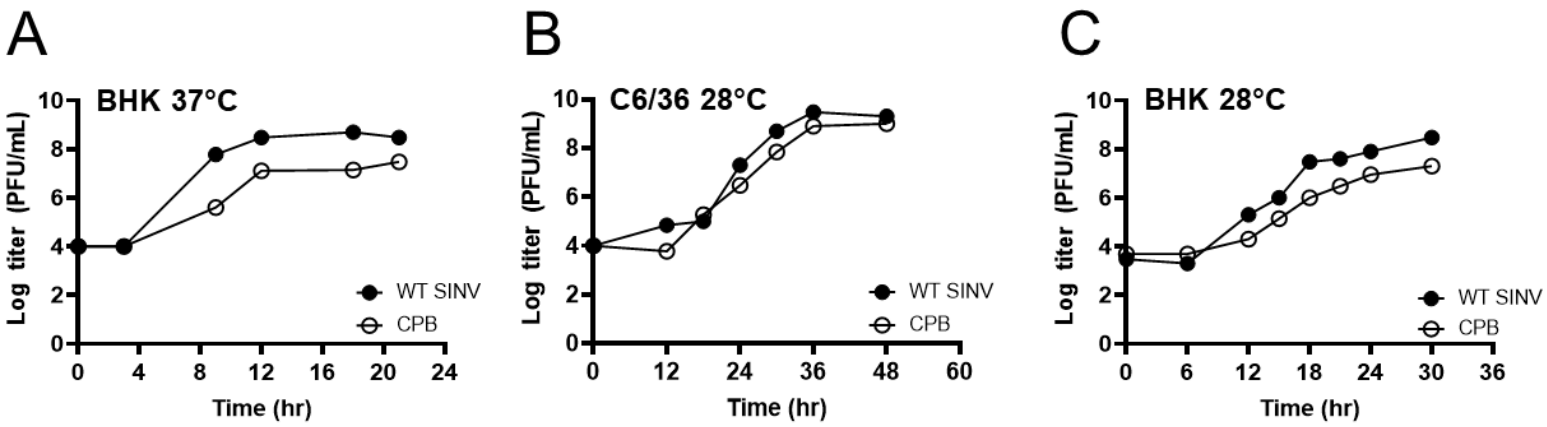
A
BHK 37°C
Log titer (PFU/mL)
Time (hr)
WT SINV
CPB
B
C6/36 28°C
Log titer (PFU/mL)
Time (hr)
WT SINV
CPB
C
BHK 28°C
Log titer (PFU/mL)
Time (hr)
WT SINV
CPB

Fig 3

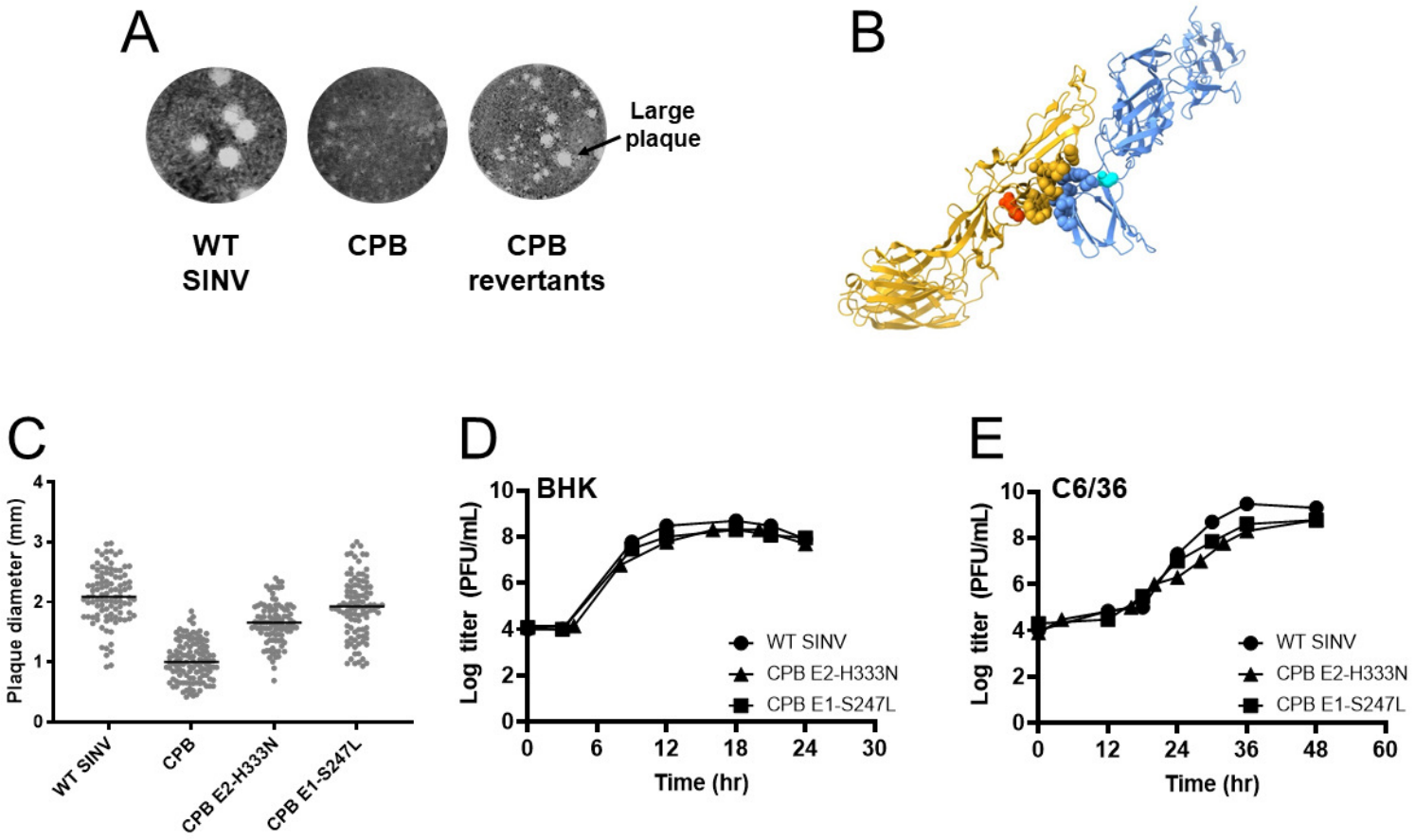
A
Large plaque
WT SINV
CPB
CPB revertants
B
C
Plaque diameter (mm)
WT SINV
CPB
CPB E2-H333N
CPB E1-S247L
D
BHK
Log titer (PFU/mL)
Time (hr)
WT SINV
CPB E2-H333N
CPB E1-S247L
E
C6/36
Log titer (PFU/mL)
Time (hr)
WT SINV
CPB E2-H333N
CPB E1-S247L

Fig 4
A, B

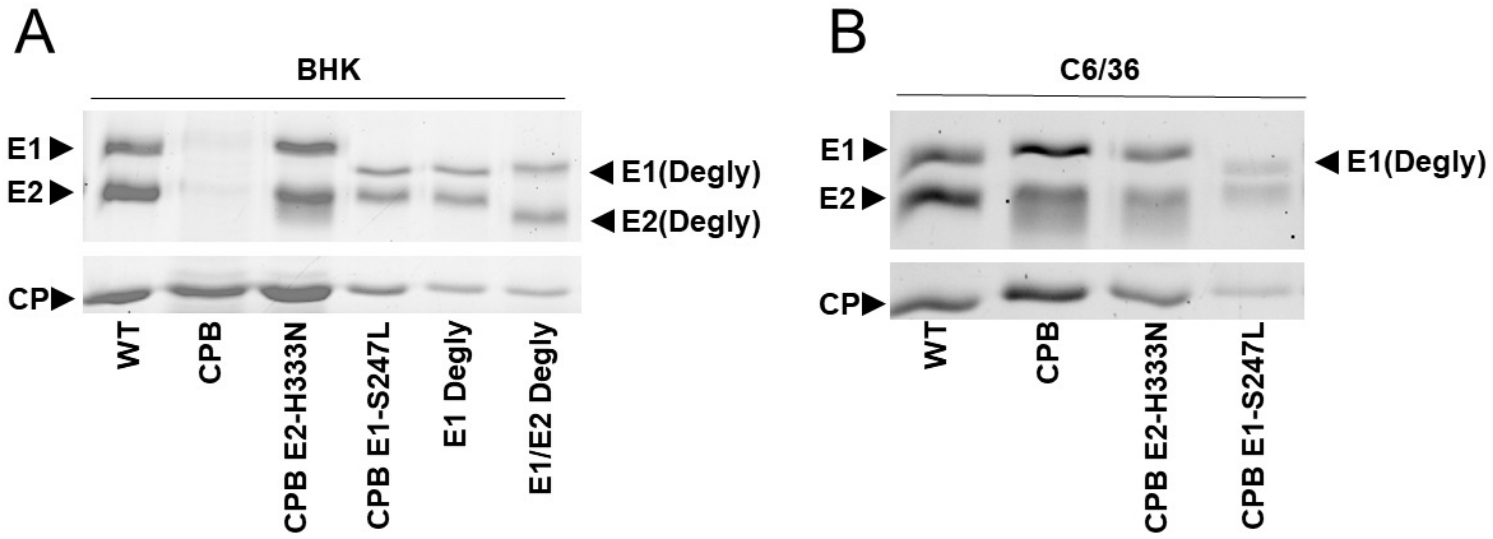
A
BHK
E1
E2
E1(Degly)
E2(Degly)
CP
WT
CPB
CPB E2-H333N
CPB E1-S247L
E1 Degly
E1/E2 Degly
B
C6/36
E1
E2
E1(Degly)
CP
WT
CPB
CPB E2-H333N
CPB E1-S247L

Fig 4
C, D

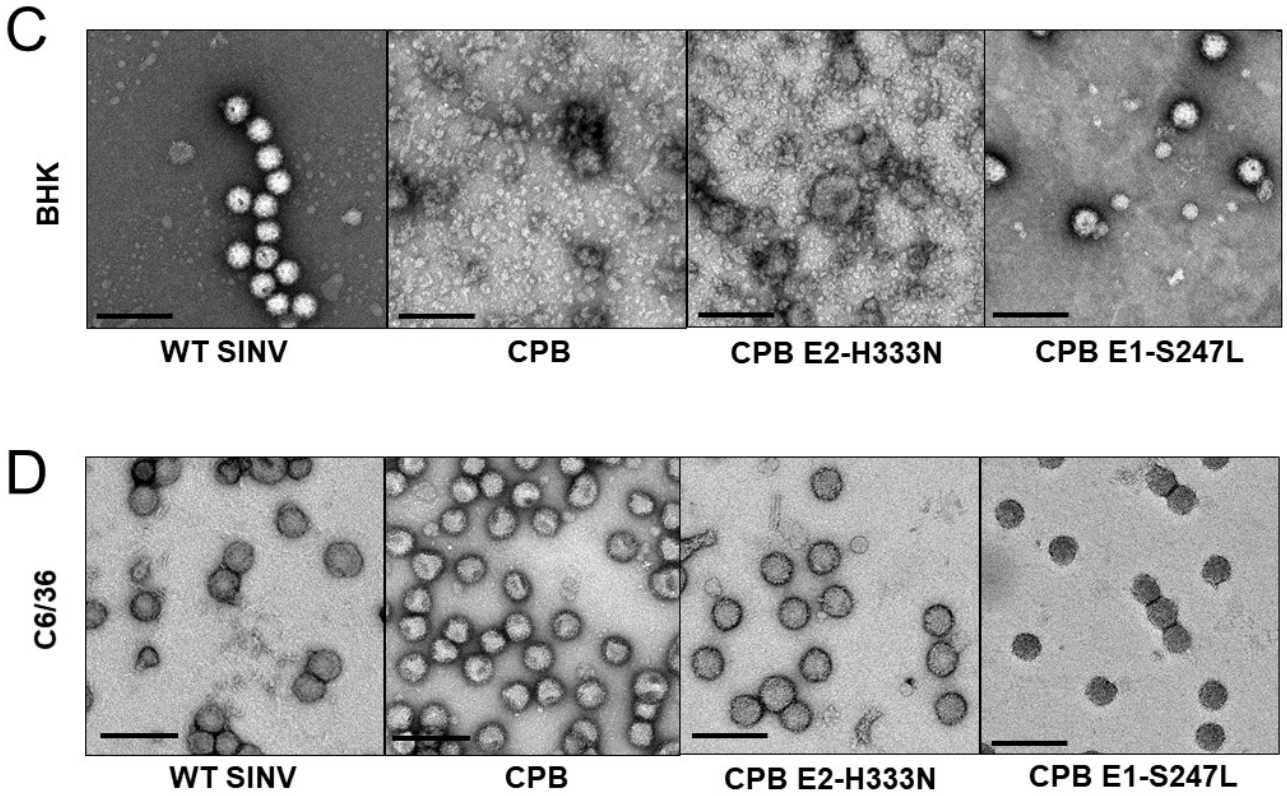
C
BHK
WT SINV
CPB
CPB E2-H333N
CPB E1-S247L
D
C6/36
WT SINV
CPB
CPB E2-H333N
CPB E1-S247L

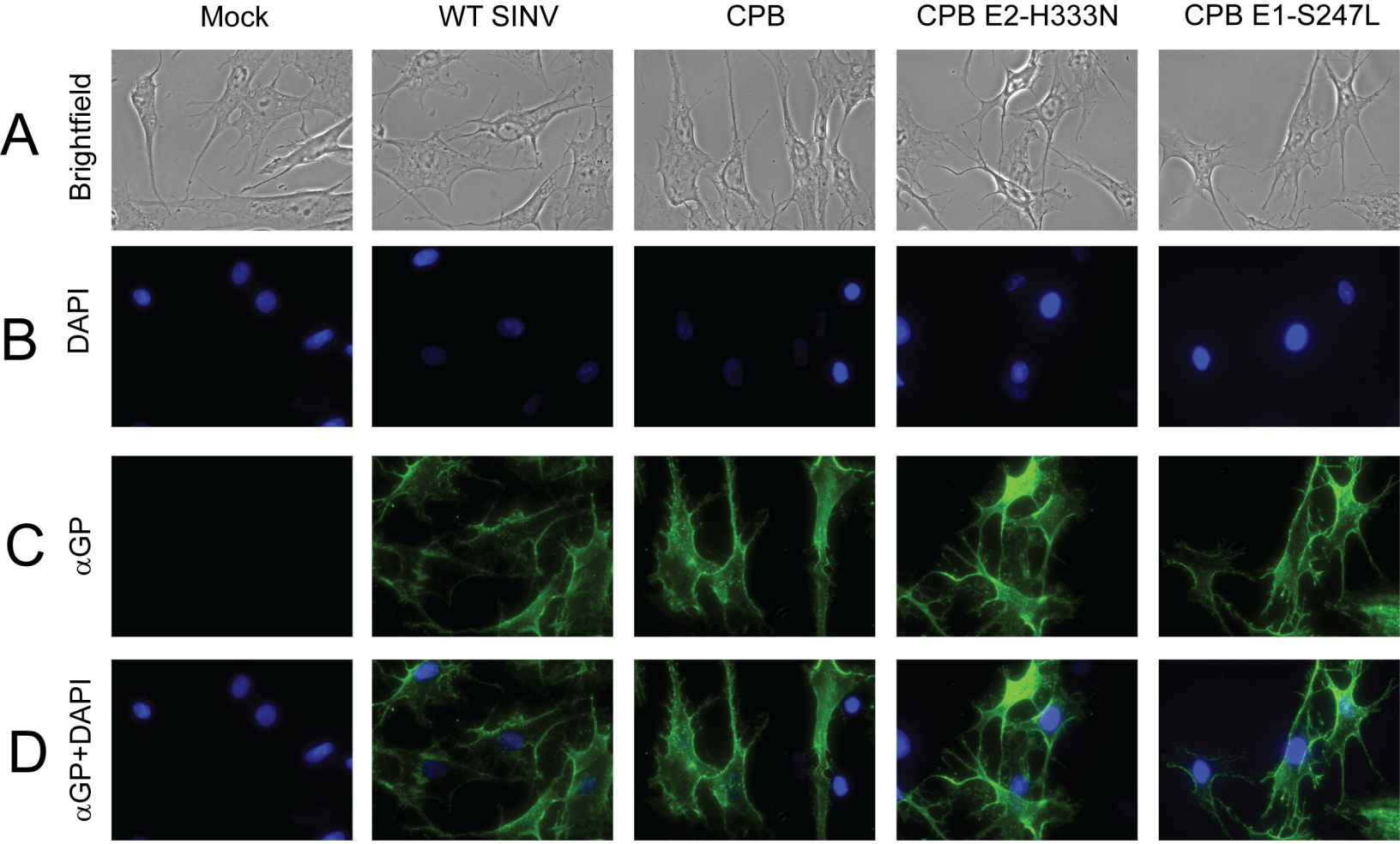
Mock
WT SINV
CPB
CPB E2-H333N
CPB E1-S247L
A
Brightfield
B
DAPI
C
αGP
D
αGP+DAPI

Fig 6, A-F

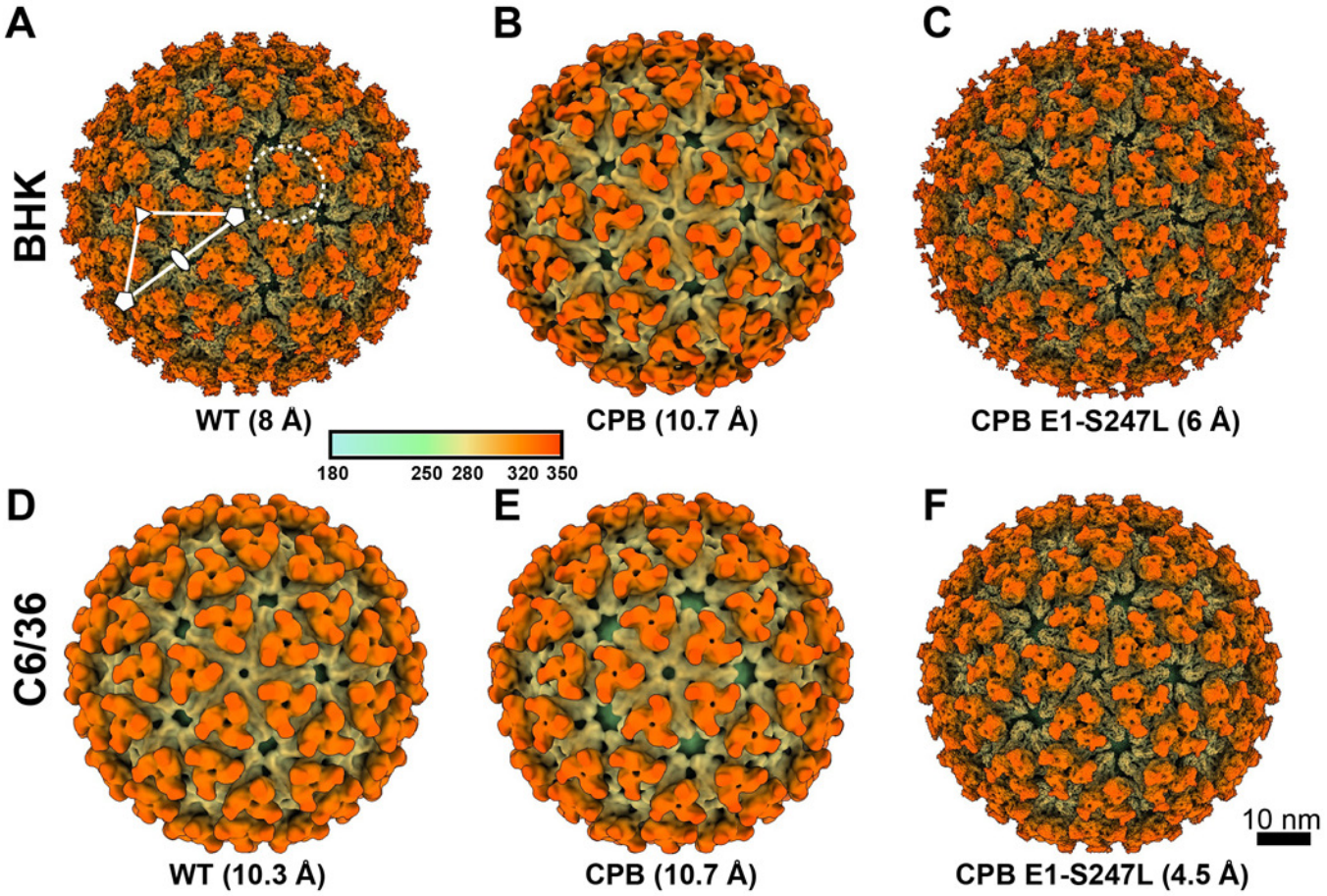
A
B
C
BHK
WT (8 Å)
CPB (10.7 Å)
CPB E1-S247L (6 Å)
180
250 280
320 350
D
E
F
C6/36
WT (10.3 Å)
CPB (10.7 Å)
CPB E1-S247L (4.5 Å)
10 nm

Fig 6,
G-L

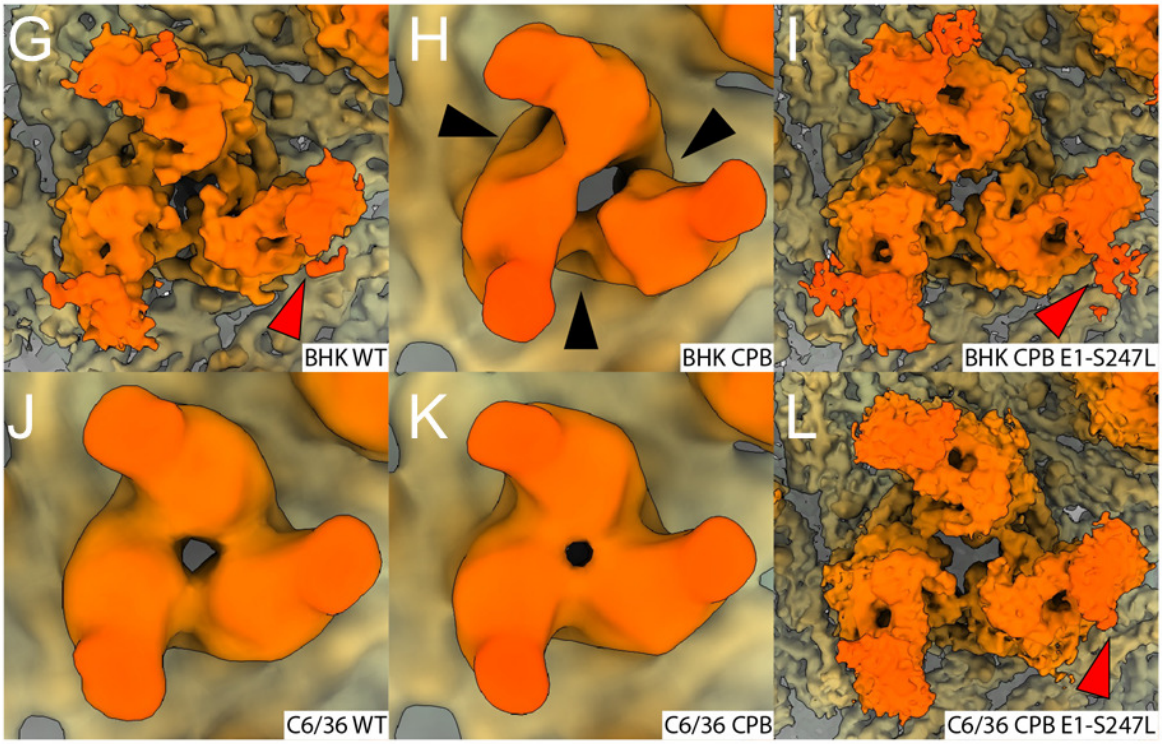
G
BHK WT
H
BHK CPB
I
BHK CPB E1-S247L
J
C6/36 WT
K
C6/36 CPB
L
C6/36 CPB E1-S247L

Table 1: Location of glycosylation sites

Virus	Protein	Glycosylation site
SINV	E2	N196
SINV	E2	N318
SINV	E1	N139
SINV	E1	N245
CHIKV	E2	N263
CHIKV	E2	N345
CHIKV	E1	N141

Reconstruction data	WT SINV (BHK)	CPB (BHK)	CPB E1-S247L (BHK)	WT SINV (C6/36)	CPB (C6/36)	CPB E1-S247L (C6/36)
Data collection information						
Electron microscope	TFS Titan Krios	TFS Titan Krios	TFS Titan Krios	JEOL 3200FS	TFS Titan Krios	TFS Titan Krios
Operation voltage (kV)	300	300	300	300	300	300
Electron detector	Gatan K3	Gatan K3	Gatan K3	DE-12	Gatan K3	Gatan K3
Energy filter (slit width in eV)	20	20	20	20	20	20
Data collection mode	Counting	Super-resolution counting	Counting	Integrated	Counting	Counting
Nominal magnification	105,000x	64,000x	64,000x	80,000x	64,000x	64,000x
Pixel size in 3D map (Å) (Pixel size in the censor)	1.68 (0.84)	2.72 (0.68)	1.36 (1.36)	1.9 (1.9)	2.72 (1.36)	1.36 (1.36)
Total accumulated dose (e^-/ $Å^2$)	30	30	30	30	30	30
Data process statistics						
Box size (pixel)	500	300	600	440	300	600
Number of particles	9037	15956	16133	7102	63509	65053
CTF estimation	CTFFIND4	CTFFIND4	CTFFIND4	CTFFIND4	CTFFIND4	CTFFIND4
Data processing software	RELION 3.1	RELION 3.1	RELION 3.1	RELION 3.1	RELION 3.1	RELION 3.1
Symmetry imposition	I2	I2	I2	I2	I2	I2
B-factor applied ($Å^2$)	-545.7	N/A	-311.4	-297.3	N/A	-237.3
Final resolution (Å)	8	10.7	5.9	10.3	10.7	4.5